HHS Public Access

Author manuscript

Eur J Nucl Med Mol Imaging. Author manuscript; available in PMC 2018 March 01.

Published in final edited form as:

Eur J Nucl Med Mol Imaging. 2017 March ; 44(3): 517–532. doi:10.1007/s00259-016-3560-9.

Lymphoma: current status of clinical and preclinical imaging with radiolabeled antibodies

Christopher G. England[1], **Lixin Rui**[2,3], and **Weibo Cai**[1,3,4]

[1]Department of Medical Physics, University of Wisconsin School of Medicine and Public Health, 1111 Highland Ave, Madison, WI 53705-2275, USA

[2]Department of Medicine, University of Wisconsin School of Medicine and Public Health, Madison, WI, USA

[3]Carbone Cancer Center, University of Wisconsin School of Medicine and Public Health, Madison, WI, USA

[4]Department of Radiology, University of Wisconsin School of Medicine and Public Health, Room 7137, 1111 Highland Ave, Madison, WI 53705-2275, USA

Abstract

Lymphoma is a complex disease that arises from cells of the immune system with an intricate pathology. While lymphoma may be classified as Hodgkin or non-Hodgkin, each type of tumor is genetically and phenotypically different and highly invasive tissue biopsies are the only method to investigate these differences. Noninvasive imaging strategies, such as immunoPET, can provide a vital insight into disease staging, monitoring treatment response in patients, and dose planning in radioimmunotherapy. ImmunoPET imaging with radiolabeled antibody-based tracers may also assist physicians in optimizing treatment strategies and enhancing patient stratification. Currently, there are two common biomarkers for molecular imaging of lymphoma, CD20 and CD30, both of which have been considered for investigation in preclinical imaging studies. In this review, we examine the current status of both preclinical and clinical imaging of lymphoma using radiolabeled antibodies. Additionally, we briefly investigate the role of radiolabeled antibodies in lymphoma therapy. As radiolabeled antibodies play critical roles in both imaging and therapy of lymphoma, the development of novel antibodies and the discovery of new biomarkers may greatly affect lymphoma imaging and therapy in the future.

Keywords

Molecular imaging; Non-Hodgkin lymphoma; Hodgkin lymphoma; Cancer imaging; Positron emission tomography; Radioimmunotherapy

Correspondence to: Christopher G. England; Weibo Cai.

Conflicts of interest None.

Ethical approval This article does not describe any studies with human participants or animals performed by any of the authors.

Introduction

Lymphoma is an umbrella term that encompasses a large group of cancers that often arise from the lymph nodes [1]. In the nodes, lymphocytes undergo mutations or changes that result in uncontrollable cell proliferation, ultimately leading to tumorigenesis. While the cause of lymphoma remains unknown, certain individuals are more susceptible to developing the disease, including HIV-positive patients and people infected with several other viruses or bacteria including *Helicobacter pylori*, Epstein-Barr virus, and human T-lymphotropic virus [2]. Also, some studies have suggested a genetic link or familial connection in lymphoma development [3]. The classification of lymphoma is complex, yet can be divided into two general categories, including non-Hodgkin lymphoma (NHL) and Hodgkin lymphoma (HL). However, these two categories can be further organized into more than 30 types of NHL and five types of HL, which are outlined in Table 1. For more information on the types of lymphoma, readers are directed to excellent review articles on this topic [4–7]. When caught early, lymphoma is highly treatable and often curable. For this reason, novel tools for diagnostic imaging and therapeutic monitoring can provide insight into early disease detection, development of new and existing treatment regimens, and potential patient stratification.

Treatment of lymphoma is dependent upon several factors, including the classification, disease grade, biomarker expression, and general health of the patient [8]. Therapeutic intervention may consist of chemotherapy, radiation therapy, and immunotherapies, radioimmunotherapy (RIT), interleukin-2 and vaccines; and stem cell transplants and surgical intervention may be viable options in patients with recurrent disease (Fig. 1). For NHL, CHOP-R (cyclophosphamide, doxorubicin, vincristine and prednisone in combination with rituximab) is standard first-line therapy in Europe [9, 10]. There are several other chemotherapy regimens that have been used successfully for treating lymphoma. In patients with larger lymph nodes or localized disease, external beam radiation therapy is a viable treatment option [11]. Another treatment option is immunotherapy, which utilizes a patient's own immune system to combat cancer by producing an adaptive immune response to the tumor cells [12]. Recently, Zappasodi et al. provided a detailed review of the current status of lymphoma immunotherapy [13]. As an alternative approach for highly recurrent or progressive disease, stem cell or bone marrow transplantation may be performed, yet transplants are risky with 1-year mortality rates between 40 % and 50 % [14].

The clinical manifestations of lymphoma vary among patients depending on the organs affected by the disease, the speed of tumor growth, and the location of lymphomatous cells [15]. Patients commonly present with peripheral swollen lymph nodes in the neck, groin, or underarms [16]. Patients with intermediate or high-grade lymphoma may experience other systemic symptoms, including high-grade fevers, night sweats, weight loss, and fatigue [17–19]. Diagnosing lymphoma relies upon the expertise of internal medicine physicians, oncologists, and pathologists. While molecular imaging strategies make it possible to image lymphoma noninvasively, tissue biopsies are the only definitive method for diagnosing HL and NHL [20]. In addition to biopsies, flow cytometry and bone marrow aspiration may be used to help detect lymphoma [21, 22]. Upon diagnosis of lymphoma, patients will undergo a series of medical tests to examine further the specific disease, which may include

immunohistochemistry, cytogenetic analysis, immunophenotyping, and fluorescence in situ hybridization [23–25].

Currently, positron emission tomography (PET) imaging plays a pivotal role in staging of lymphoma in patients, helping physicians to determine the most efficient treatment options while minimizing potential toxicities. Single photon emission computed tomography (SPECT) imaging with ^{67}Ga was traditionally employed for evaluating lymphoma, yet this tracer has been widely replaced by ^{18}F-FDG (or FDG) [26]. While FDG is an effective PET tracer that enables the detection of most malignancies, it is limited by nonspecific uptake in nonmalignant tissues (e.g. inflammatory tissues). Also, FDG provides no phenotypic information about the tumor; thus, highly invasive tissue biopsies are required to determine the tumor phenotype, which guides the choice of therapy in a particular patient. As a means to compensate for the limitations of FDG PET, immunoPET imaging has been evaluated for preclinical imaging of lymphoma. By utilizing the high specificity and avidity of antibodies, antibody-based imaging agents can allow effective visualization of lymphoma in vivo. ImmunoPET imaging has become a vital part of preclinical research, as it allows researchers to investigate the unique phenotype of tumors, which may augment the diagnosis, therapeutic intervention strategies, and monitoring of therapeutic response in patients with lymphoma [27].

This review examines the current status of immunoPET imaging for lymphoma, including both preclinical and clinical imaging research. In the next section we provide a historical overview and discuss the current status of clinical lymphoma. We then provide a thorough investigation into the preclinical imaging of lymphoma, offering an insight into the various preclinical mouse models of lymphoma available for imaging-related studies, the two biomarkers commonly used for preclinical immunoPET imaging of lymphoma (CD20 and CD30), and the application of immunoPET agents for imaging lymphoma in patients. As radiolabeled antibodies play a vital role in lymphoma treatment, this topic is also briefly examined. Lastly, we discuss potential pitfalls and improvements that may be addressed to advance the clinical translation of radiolabeled antibodies for imaging of lymphoma in the future.

Clinical imaging of lymphoma: historical overview and current status

Since lymphoma elicits few symptoms in patients, diagnosing the disease can be difficult. Noninvasive imaging modalities can be used to screen patients with suspected lymphoma. Clinical imaging of lymphoma provides the necessary information to stage the disease and monitor treatment response. Before the advent of FDG PET, computerized axial tomography (CT) was the sole imaging modality used for evaluating lymphoma in patients. While the disease can be staged in most patients, the low specificity of CT inhibits the detection of cancer in lymph nodes of normal size. In addition, CT cannot distinguish between tumor and fibrotic tissue induced by anticancer treatment. Multidetector-row CT, that was introduced in the late 1990s, can image thinner slices of tissue rapidly, allowing the detection of lymph nodes <5 mm in size, while also minimizing breathing artifacts [28]. Currently, multidetector-row CT scanners with at least four sections are used for staging of malignant lymphoma in patients after injection of iodinated contrast medium. Despite significant

improvements in CT, this imaging modality is limited by its low specificity, the requirement for ionizing radiation exposure, the possible elicitation of an allergic reaction to the iodinated contrast agent, and the fact that it does not provide any functional or metabolic information about the tumor [29–32].

In the past, the standard tracer for imaging lymphoma was ^{67}Ga citrate. The first use of ^{67}Ga for lymphoma imaging was reported in 1969 [33–35]. In clinical trials, ^{67}Ga citrate yielded an overall accuracy of 83 % in the detection of both HL and NHL by scintigraphy [36]. ^{67}Ga citrate localizes in the tumor through targeting of transferrin-binding receptors upregulated on tumor cells [37]. Although it is an effective tracer, the ability of ^{67}Ga to detect malignancies below the diaphragm is limited by its hepatic clearance [38]. In addition, the tracer displays low specificity, accumulating in both malignant and inflammatory tissues [39]. In combination with SPECT, ^{67}Ga citrate can detect 93 % of lymphoma tumors in patients [40]. The clinical availability of hybrid imaging modalities, combining CT with SPECT(SPECT/CT) or PET (PET/CT), have significantly improved the diagnosis of many cancers, including lymphoma [41]; yet, imaging with ^{67}Ga citrate has been widely replaced by FDG PET imaging, which has fast acquisition times with high spatial resolution [42].

In 1987, the first study was published investigating the clinical use of FDG PET for imaging of lymphoma [43], and by the late 1990s ^{18}F-FDG had been extensively evaluated for the staging of lymphoma [44]. In comparisons of FDG PET and ^{67}Ga scintigraphy in the imaging of both HL and NHL, FDG PET consistently showed higher sensitivity than ^{67}Ga scintigraphy [45–48]. In the late 1980s, the uptake of these two tracers was compared in five patients with NHL (the scans in two of these patients, patients 1 and 4, are shown in Fig. 2) [43]. Patient 1 was a 26-year-old man with a palpable tumor in the upper left quadrant of the abdomen, which was found to be a large tumor at laparotomy. While the ^{67}Ga scan was normal, the ^{18}F-FDG scan showed accumulation of the tracer in this region. Patient 4 presented with large lymph nodes in his neck and groin (Fig. 2). Biopsy of the biggest cervical lymph node confirmed that the disease was diffuse small lymphocytic lymphoma. While the ^{67}Ga scan clearly showed the cervical lymph nodes, ^{18}F-FDG allowed better delineation of the involvement of the inguinal lymph nodes due to its high sensitivity. Since that time, FDG PET images have significantly improved and ^{18}F-FDG has become the standard tracer for imaging lymphoma and most other cancers [49]. When compared to CT imaging, FDG PET has continually shown superiority in monitoring treatment response in patients with lymphoma and in predicting progression-free survival in patients [50, 51]. FDG has been shown to have high avidity for HL and some forms of NHL in the range 97 – 100 % [30]. However, some forms of NHL show low FDG avidity, including mucosa-associated lymphoid tissue (MALT) marginal zone lymphoma (54 – 81 %), small lymphocytic lymphoma (47 – 83 %), marginal zone lymphoma (53 – 67 %), primary cutaneous anaplastic large T cell lymphoma (40 – 60 %), and others (Table 2).

Dual-modality PET/CT scanners provide additive benefits. While PET imaging with ^{18}F-FDG shows the tissues undergoing high levels of glycolysis, CT imaging provides an anatomical reference to register the PET images spatially and enables attenuation correction, which improves overall quantitative accuracy [52]. Also, FDG PET/CT imaging assists in radiation treatment planning, helping to minimize potential radiation exposure to healthy

tissues [53]. Currently, FDG PET/CT is recommended for the staging of lymphoma in clinical practice to determine the best site for biopsy [30]. However, it is not ordinarily recommended in patients with low avidity types of lymphoma. Additionally, FDG PET/CT is recommended for imaging during treatment to evaluate therapeutic efficacy and for posttreatment imaging to assess remission [30].

As an alternative modality for imaging lymphoma, magnetic resonance imaging (MRI) is commonly used in pediatric patients as it does not expose the patient to ionizing radiation [54]. Also, the enhanced soft tissue contrast of MRI is useful in staging lymphoma tumors that involve the spinal cord or thorax [55]. Diffusion-weighted imaging, a functional MRI protocol that examines the mobility differences between water molecules found in different tissues, has shown high sensitivity (>97 %) in staging lymphoma [56–58]. While MRI is a viable option when additional imaging studies are needed, ^{18}F-FDG PET remains the gold standard for cancer imaging.

Preclinical imaging of lymphoma using radiolabeled antibodies

Currently, the clinical imaging strategies for lymphoma fail to provide phenotypic information about the tumor. ImmunoPET imaging has become a leading contender in the field of molecular imaging, playing a significant role in the preclinical detection and staging of lymphoma. In this section the preclinical animal models commonly used in lymphoma imaging studies are discussed, including transgenic and xenograft mouse models. The recent advances in immunoPET imaging of CD20 and CD30 expression in lymphoma are summarized and the current status of radiolabeled antibodies for imaging of lymphoma in patients is discussed. While other antigens have been targeted in lymphoma, they have been primarily studied for use in RIT. These targets, including CD22 and CD37, are discussed in the section “Beyond imaging: lymphoma therapy using radiolabeled antibodies”.

Animal models of lymphoma for preclinical imaging studies

Transgenic models of lymphoma—Due to the advent of genetic engineering, there are several murine transgenic models of lymphoma readily available to researchers. Transgenic mouse models of lymphoma can recapitulate the common genetic variations found in human lymphomas, providing a realistic disease model. There are several types of genes that can be modified to produce lymphoma in mice, which may include transcription factors, cell-cycle regulators, antioncogenes, antiapoptosis genes, growth factors, receptors, and protein-modifying enzymes [59]. Transgenic mice with altered c-Myc and Bcl-2 proteins are commonly utilized for studying high-grade lymphoma [60, 61]. While it is beyond the scope of this review to describe all the transgenic mouse models of lymphoma, we briefly describe some common strains.

In the early 1980s, the critical oncogenic event that leads to the development of Burkitt lymphoma was found to be a chromosomal translocation of the c-*MYC* oncogene to within or next to an immunoglobulin heavy chain gene [62]. c-Myc is a transcription factor protein that contributes to several cellular processes, including cell proliferation, cellular metabolism, and apoptosis. This translocation causes the c-Myc protein to become overexpressed, which eventually leads to B cell tumorigenesis [63]. At a similar time, Taub

et al. discovered that a translocation placing the c-*MYC* gene within close range of Eμ, an immunoglobulin heavy chain enhancer, results in murine plasmacytoma [64]. This led to the discovery of the Eμ-Myc transgenic model, which rapidly develops lymphoma with only 10 % of mice surviving past 5 months of age [65, 66]. The tumors are malignant and highly aggressive with the vast majority being pre-B-lymphomas (52 %). While nearly 100 % of mice eventually develop lymphoma, the rate of development can be modified by inserting the oncogene at different locations in the enhancer region [66, 67].

The *BCL2* proto-oncogene produces the membrane-associated protein found in the mitochondrial and endoplasmic reticulum membranes, known as Bcl-2 [68]. This protein plays a unique role in lymphomagenesis, acting as a positive regulator of cell death. Bcl-2 was defined as an apoptosis inhibitor, and was found to cooperate with c-Myc in immortalization of pre-B cells [69]. In transgenic mice, the simultaneous overexpression of Bcl-2 and c-Myc proteins yields a synergistic effect that leads to the production of more lymphoid tumors than in transgenic mice with single *BCL2* or c-*MYC* [70, 71]. There are several co-transgenic murine models used to study lymphoma, including the blastoid variant of mantle cell lymphoma, which is investigated using cotransgenic mice expressing Myc and IL-14α [72]. A murine model of diffuse large B cell lymphoma has recently been developed by introducing the full genome of the hepatitis C virus into CD19-expressing cells [73]. Thymic lymphoma has been recreated in mice by altering *Atm* and *Prkdc* to produce 129S6/SvEvTac-Atm^{tm1Awb} and NOD.Cg-Prkdc^{scid} Emv30^{b}/Dvs, respectively [74]. Also, T cell lymphoma has been successfully recreated in many T cell prone mouse strains, including C548, HRP, and AKR. For more information regarding transgenic murine models of lymphoma, readers are directed to an excellent review covering this topic [75].

Human tumor xenograft models of lymphoma—Human tumor xenografts are the most common murine model of lymphoma used for preclinical research. In comparison to other cancers, lymphoma is among the most difficult types of tumor to grow in nude mice due to macrophage activity, enhanced natural killer (NK) cell activity, and the production of antibodies [76, 77]. Several strategies have been employed to improve xenograft take rates in athymic nude mice, including whole-body irradiation, antithymocyte or antilymphocyte serum administration, injection of cyclophosphamide, and splenectomy [78, 79]. While these methods improve the establishment of xenograft tumors in athymic nude mice, which have normal B cell and NK-cell activity, more immunodeficient models have simplified the process of xenograft implantation of lymphoma tumors.

The murine C.B-17 severe combined immunodeficiency (SCID) strain lacks both T cell and B cell activity [80]. Also, this strain of mouse is also deficient in immune effector functions; thus, the SCID model has become widely employed for implantation of lymphohematopoietic tumors. The advent of obese/nonobese (NOD) SCID mice improved upon the immunodeficiency of C.B-17 SCID strain as it is deficient in both T cell and B cell activity, yet is also deficient in NK cell activity and lacks serum immunoglobulins [81]. While this animal is optimal for lymphoma xenograft implantation, the high price and short lifespan (about 8 months) of these mice effectively limit their extensive use in research.

While most xenografts are implanted using lymphoma cell lines, patient-derived xenografts have become popular for research purposes. In this situation, lymphoma tissue is excised from the patient and homogenized into a cell suspension for injection into the mice or surgically transplanted into the mice [82]. While the patient-derived xenograft better represents the tumors found in patients, their heterogeneous structure makes them difficult to treat and target for imaging-related studies. For this reason, most xenograft models rely upon highly homogeneous cell cultures. Lymphoma cells may be injected into mice via several routes, with subcutaneous and orthotopic implantation being customary. Some of the common lymphoma cell lines used to create xenograft models include Raji and Ramos for Burkitt's lymphoma, FL-18 for follicular small cleaved cell lymphoma, and Karpas 299 for anaplastic large cell lymphoma. Other common lymphoma cell lines are listed in Table 3.

A current limitation of the human xenograft model is that it does not recapitulate the immune system found in patients. The complex interactions between cancer and immune cells are of great interest in therapeutic and imaging studies. Since lymphoma is a cancer that arises directly from immune cells, these animal models provide limited data on lymphoma, bringing into question the clinical relevance of this model. To overcome this limitation, researchers have employed humanized mouse models. The development of humanized mouse models has been reviewed [83]. Briefly, humanized mouse models are created by engrafting human immune cells into highly immunodeficient mice. There are several types of mice that have been created through this process, including Hu-PBL-SCID, Hu-SRC-SCID, and SCID-Hu. First, Hu-PBL-SCID (PBL model) mice are injected with human peripheral blood mononuclear cells (hPBMCs) [84]. These mice eventually succumb to graft versus host disease, which limits their use to only 4 to 6 weeks after injection of hPBMCs [85]. Next, Hu-SRC-SCID mice are sublethally irradiated and injected with hematopoietic stem cells. The SCID-Hu mice are coimplanted with human fetal liver and thymus tissues under the renal capsule after sublethal irradiation, along with autologous CD34+ hematopoietic stem cells. Also known as the BLT model, these mice develop a robust immune system with sustained levels of Tcell development [86]. In addition, it is possible to detect both T- and B cell response to infections in these mice, making this model the best humanized model for interactions between the immune system and similar diseases.

Preclinical imaging of CD20 in lymphoma using radiolabeled antibodies

CD20 is an antigen expressed on the surface of mature and malignant B cells mediating B cell activation and proliferation. It is widely expressed in many B cell malignancies, including B cell lymphoma and B cell chronic lymphocytic leukemia [87, 88]. CD20 expression has also been found in some forms of HL [89]. While the expression of some surface proteins can provide prognostic information in patients, expression of CD20 does not correlate with disease severity or patient prognosis. Due to its high expression in various cancers and diseases, several antibodies targeting CD20 have been developed, including obinutuzumab, rituximab, ocaratuzumab, ocrelizumab, and veltuzumab [90]. Rituximab was the first monoclonal antibody approved in 1997 for the treatment of CD20-expressing lymphoma in the US [91, 92].

While rituximab has been used for lymphoma treatment for nearly two decades, its potential as an imaging agent has only recently been investigated. Natarajan et al. developed an immunoPET imaging agent targeting CD20 by radiolabeling rituximab with the long-lived isotope ^{89}Zr using the chelator desferrioxamine (Df) to form ^{89}Zr-Df-rituximab [93]. Due to their large size, whole antibodies require several days to achieve optimal tumor retention; thus, the long half-life of ^{89}Zr (78.4 h) is ideal for investigating the long-term biodistribution of antibodies in vivo [94]. To examine the biodistribution of ^{89}Zr-Df-rituximab, a transgenic mouse model was used that contains B cells expressing human CD20 as a representative model of B cell lymphoma [93]. To validate the high specificity of the tracer, one group of mice received 2 mg/kg predoses of rituximab to block the receptor and another group received no blocking. The spleen, which is rich in CD20-expressing B cells, showed enhanced tumor uptake of tracer in mice without receptor blocking, but showed significantly lower uptake in mice with blocking (Fig. 3a). A region-of-interest analysis of PET images showed that tracer accumulation was much higher in mice without blocking (83.3 ± 2.0 %ID/g) than in mice with blocking (3.2 ± 0.1 %ID/g) at 120 h after injection (Fig. 3b). In addition, the liver also showed a significant difference in uptake of tracer, yet the uptakes were low in both groups of mice (0.61 ± 0.001 %ID/g with blocking, 1.32 ± 0.05 %ID/g without blocking; Fig. 3b). Recently, the same group performed a radiation dosimetry study of ^{89}Zr-Df-rituximab, and identified 145 MBq as the human patient whole-body dose per annum that can be injected without exceeding the approved maximum permissible dose limit [95]. Also, the spleen was determined to be the dose-limiting organ in the mice without blocking, while the liver was the dose-limiting organ in the mice with blocking. Later, ^{89}Zr-labeled rituximab was used in the same laboratory for Cerenkov luminescence imaging to validate the PET findings [96].

In addition to ^{89}Zr, rituximab has also been radiolabeled with ^{64}Cu for PET imaging of lymphoma utilizing the same transgenic animal model with human CD20-expressing B cells [97]. The antibody was conjugated to the chelator tetraazacyclododecane-1,4,7,10-tetraacetic acid (DOTA), which allows effective chelation of ^{64}Cu. Due to the short half-life of ^{64}Cu (12.7 h), the biodistribution of the tracer (^{64}Cu-DOTA-rituximab) was monitored for only 48 h. The spleen could be easily delineated at 24 h after injection in mice without blocking (16.5 ± 0.45 %ID/g), and the mice with blocking showed minimal uptake (16.5 ± 0.45 %ID/g). In addition, rituximab has also been labeled with ^{99m}Tc for SPECT imaging [98] and the near-infrared dye Cy5.5 for optical imaging [99].

To further enhance the pharmacokinetic properties of rituximab, Olafsen et al. developed several anti-CD20 antibody fragments as potential imaging agents for NHL [100, 101]. For example, they created a recombinant 80-kDa minibody of rituximab and radiolabeled it with ^{64}Cu for imaging of CD20 expression in lymphoma tumor-bearing mice [100]. Highly specific tumor uptakes were observed in the CD20-positive subcutaneous xenograft model (about 11.5 %ID/g at 4 h after injection), while the CD20-negative tumors showed significantly lower uptake at the same time point. The same group also designed five CD20 diabodies for detection of low-grade B cell lymphoma by radiolabeling the antibody fragments with ^{124}I for PET imaging [101]. Tracer uptake was significantly higher at 8 h after injection in nude mice implanted with CD20-transfected lymphomatous B cells (2.2 ± 0.6 %ID/g) than in mice implanted with untransfected cells (1.0 ± 0.4 %ID/g). While the

tracer uptake was lower than with full antibodies, the pharmacokinetics of this tracer would allow same-day imaging in patients. In addition to single-modality imaging agents, the advent of dual-modality imaging agents has allowed monitoring of disease progression using several imaging modalities. For example, Paudyal et al. designed a dual PET/optical agent for imaging of CD20 expression in SCID mice bearing CD20-expressing Raji xenograft tumors [102]. The anti-CD20 antibody (NuB2) was first conjugated with Alexa Fluor 750 before being radiolabeled with ^{64}Cu through DOTA. The dual-labeled antibody showed high uptake in the tumors by 24 h after injection (16.34 ± 2.75 %ID/g), but these results are difficult to compare regarding specificity as the study lacked a CD20-negative xenograft model or in vivo blocking study.

The long blood circulation half-life of full antibodies can potentially hinder the clinical translation of antibody-based imaging agents. While utilization of fragmented antibodies can significantly decrease the blood circulation time, allowing optimal accumulation in the tumor at 12 – 24 h after injection, these small antibody fragments undergo rapid renal filtration and clearance, which limits the overall tracer accumulation in diseased tissues. To overcome this limitation, Mendler et al. designed an anti-CD20 fragmented antibody tracer with enhanced blood circulation properties for PET imaging of CD20 expression in lymphoma [103]. First, recombinant antigen-binding fragments (Fabs) were derived from the anti-CD20 monoclonal antibody ofatumumab. To improve the pharmacokinetics and biodistribution of the Fab tracer, the Fabs were fused to long amino acid chains in a process called PASylation. The antibody fragments were radiolabeled with ^{124}I for PET imaging in CD1-Foxn1^{nu} mice bearing CD20-positive Granta human tumor xenografts to determine the optimal length of PASylation. The optimal size of the polypeptide chain was thought to be 100 amino acids, as this provided optimal tumor accumulation at 6 h after injection (8.45 ± 1.38 %ID/g), but the accumulation rapidly declined to 2.82 ± 0.58 %ID/g by 24 h after injection. Fabs conjugated to the long polypeptide chain of 400 amino acids showed lower initial tumor accumulation of 4.03 ± 0.71 %ID/g at 6 h after injection, but the tracer uptake gradually increased to 6.33 ± 1.73 %ID/g by 24 h after injection. Additionally, the 100 amino acid polypeptide chain resulted in the highest tumor to blood ratio of about 15 at 48 h after injection, which decreased as the chain size increased with a ratio of about 10 for the 200 amino acid polypeptide and a ratio of <5 for longer chains. These results show that the biodistribution of antibody fragments can be readily optimized for in vivo imaging studies, which may assist in the clinical translation of antibody-based imaging agents.

Preclinical imaging of CD30 in lymphoma using radiolabeled antibodies

The cell surface receptor CD30, also known as tumor necrosis factor receptor superfamily 8 (TNFRSF8), is a protein in the tumor necrosis factor receptor family [104]. In normal tissues, CD30 expression is primarily limited to activated B- and T cells [105]; however, overexpression of CD30 has been found in both B- and T cell lymphoma [106], along with several other malignancies [107]. In 2011, Seattle Genetics designed an antibody–drug conjugate targeting CD30 that has received FDA approval for the treatment of relapsed HL and anaplastic large cell lymphoma [108]. Brentuximab vedotin was constructed by connecting an anti-CD30 antibody to the anticancer agent monomethyl auristatin E (MMAE) using a specialized linker that can be selectively cleaved by lysosomal proteases

once inside the cell to release the MMAE for therapeutic action. Inside the cell, MMAE binds to tubulin and induces cell cycle arrest through the G2/M phases, effectively resulting in apoptosis [109]. There has been extensive research verifying the enhanced expression of CD30 in B cell, T cell and NK cell lymphomas [110–112]; thus, CD30 imaging agents may be useful for the clinical imaging of several types of lymphoma in the future.

Recently, Moss et al. investigated brentuximab vedotin as a potential PET agent for imaging of CD30 expression in lymphoma by radiolabeling the compound with ^{89}Zr [113]. Three tumor-bearing mouse xenograft models were used to determine the specificity of the tracer with Karpas 299, TF1-α and Daudi, representing high CD30 expression, low CD30 expression and CD30-negative tumor model, respectively. At 144 h after injection of ^{89}Zr-labeled brentuximab vedotin, tumor-to-muscle ratios were 15.05 and 0.90 for the Karpas 299 and TF1-α model, respectively. These results further validate the enhanced specificity of the ^{89}Zr-labeled brentuximab vedotin tracer for imaging of CD30, while also proving that the radiolabeling process has no adverse effects on the immunoreactivity or pharmacokinetics of the tracer in vivo.

In a similar study, Rylova et al. also investigated CD30 expression in lymphoma using an ^{89}Zr-labeled antibody. The tumor-targeting abilities of the murine anti-human CD30 antibody AC-10 were assessed in Balb/c nude mice bearing subcutaneous CD30-expressing Karpas 299 xenograft tumors or CD30-negative A-431 xenograft tumors [114]. First, the antibody was conjugated to the chelator Df, and flow cytometry was used to assess the binding of AC-10 and Df-AC-10 to Karpas-299 and A-431 cells (Fig. 4a). Next, cellular binding assays were used to confirm that the immunoreactivity of the antibody remained intact after conjugation and ^{89}Zr labeling of the antibody (Fig. 4b). The biodistribution of the tracer (^{89}Zr-Df-AC-10) was monitored by PET imaging and tracer uptake in the CD30-expressing xenograft tumors was determined to be 37.9 ± 8.2 %ID/g, while the CD30-negative tumor model showed significantly lower tracer uptake of only 11.0 ± 0.4 %ID/g at 72 h after injection. Even at 144 h after injection, PET/CT images showed high signal in the Karpas 299 xenograft model that allowed clear delineation of the tumor (Fig. 4c). Ex vivo histology (H&E staining) and digital autoradiography were used to verify the PET data (Fig. 4d). The radiotracer was also shown to be highly specific in blocking studies, proving that anti-CD30 tracers are promising candidates for imaging of CD30-expressing lymphoma.

Imaging of lymphoma in patients using radiolabeled antibodies

The potential clinical translation of imaging agents remains a limiting factor. While there are limited studies investigating the biodistribution of radiolabeled antibodies in lymphoma patients, several radiolabeled antibodies have shown remarkable effectiveness as RIT agents. There are two FDA-approved RIT agents targeting CD20: ibritumomab tiuxetan (Zevalin) labeled with ^{90}Y and tositumomab labeled with ^{131}I (Bexxar); the use of these agents in RIT is discussed in section “Beyond imaging: lymphoma therapy using radiolabeled antibodies” [115]. Recently, Iagaru et al. investigated the efficacy of ^{90}Y-ibritumomab tiuxetan in the treatment of NHL using ^{111}In-ibritumomab for pretreatment imaging [116]. In addition, ibritumomab tiuxetan has also been radiolabeled with ^{89}Zr for quantifying the biodistribution and dosimetry of ^{90}Y-ibritumomab tiuxetan in patients with NHL [117, 118].

Both ^{18}F-FDG and ^{89}Zr-ibritumomab tiuxetan allow delineation of the malignancies in NHL patients, showing the cervical, mediastinal, left caput humeri, splenic, para-aortic, and inguinal lymph node lymphomas, as shown in Fig. 5a [117]. However, ^{89}Zr-ibritumomab tiuxetan also showed high uptake in the liver which was attributed to nonspecific retention of ^{89}Zr after catabolism of the antibody conjugate (Fig. 5b).

In another study, Rizvi et al. used ^{89}Zr-ibritumomab tiuxetan to assess the biodistribution of ^{90}Y-ibritumomab tiuxetan in humans [118]. The objective was to determine if coinjection of a therapeutic dose of ^{90}Y-ibritumomab tiuxetan would significantly alter the biodistribution of ^{89}Zr-ibritumomab tiuxetan. The researchers found that imaging with ^{89}Zr-ibritumomab tiuxetan made it possible to predict the radiation dosimetry for ^{90}Y-ibritumomab tiuxetan treatment in NHL patients scheduled for autologous stem cell transplantation, providing further evidence that antibody-based imaging agents may be clinically utilized to investigate treatment response in patients undergoing RIT.

The anti-CD20 antibody rituximab was recently evaluated as a PET imaging agent in patients with CD20-expressing B cell lymphoma. In this study, Muylle et al. investigated the biodistribution of ^{89}Zr-labeled rituximab in patients injected with and without a preload of unlabeled rituximab to determine if preloading would affect the tumor-targeting ability or radiation dose of subsequent ^{90}Y-rituximab RIT [119]. Injection of a preload of unlabeled rituximab resulted in decreased tumor targeting of the radioconjugate in most patients, especially those patients who were B cell-depleted due to prior treatment with rituximab, such as the patient in Fig. 6 with grade II follicular lymphoma. While these studies provide evidence supporting the use of immunoPET agents for imaging lymphoma in patients, additional studies are necessary to investigate the biodistribution and pharmacokinetics of these immune-targeting antibodies in both healthy patients and patients with lymphoma.

Beyond imaging: lymphoma therapy using radiolabeled antibodies

While the primary focus of this review is radiolabeled antibodies for imaging lymphoma, the widespread use of radiolabeled antibodies for RIT of lymphoma warrants a brief discussion. Over the last two decades, RIT using radiolabeled antibodies has shown remarkable success in improving patient survival in many types of lymphoma [120]. The enhanced efficacy of RIT has been attributed to the fact that many types of lymphoma are radiosensitive and multifocal [121]. Commonly, radiolabeled antibodies for RIT are labeled with ^{90}Y for therapy or ^{131}I for therapy and imaging.

Bexxar (^{131}I-tositumomab) is a RIT agent targeting CD20 that received FDA approval in 2003 for the treatment of various forms of NHL [122]. The agent was used with success for several years after receiving FDA approval until the sales of the drug started to decline rapidly by 30 % each year. While Bexxar showed excellent efficacy and safety profiles in most clinical trials, a significant turning point was in 2011 when researchers from the Fred Hutchinson Cancer Research Center revealed the results of a large clinical trial in NHL (554 patients) that showed no significant improvements in response rates or survival rates between patients receiving Bexxar and CHOP and those receiving rituximab and CHOP

[123]. This result, in combination with its declining sales, led to discontinuation of the product by GlaxoSmithKline in 2014.

The next RIT agent used for lymphoma treatment was Zevalin, a radiolabeled antibody targeting CD20 [115]. The antibody is ibritumomab, a murine IgG1 κ class. A chelator linker (tiuxetan) is utilized to provide a high-affinity chelation site for ^{90}Y. Upon binding to CD20, the receptor remains on the surface of the cell and the therapeutic action of Zevalin is induced by the beta emission from ^{90}Y, which leads to the formation of damaging free radicals in nearby cells. Similar to Bexxar, infusion of unlabeled antibody (tositumomab for Bexxar and rituximab for Zevalin) is given before the RIT agent to significantly reduce the number of circulating B cells, thus limiting potential off-target toxicities. Currently, Zevalin is approved to treat low-grade or follicular B cell NHL that has relapsed during or after treatment with other anticancer drugs, and newly diagnosed follicular NHL that has shown an initial response to anticancer therapies.

Several other RIT agents are actively being explored as potential agents for the treatment of lymphoma. For example, epratuzumab is a humanized antibody targeting CD22, known to be highly expressed in most types of lymphoma [124]. Previously, this antibody was labeled with ^{90}Y and has been used for the treatment of aggressive NHL with 53 % of patients showing an objective response [125]. Instead of rituximab, an antibody targeting CD20 (veltuzumab) was used to decrease the amount B cells circulating in the blood. Bodet-Milin et al. evaluated the response to ^{90}Y-labeled epratuzumab in NHL patients using FDG PET (Fig. 7) [126]. FDG PET and CT imaging were performed before and after RIT. In the patient in Fig. 7, pretreatment imaging revealed the involvement of a lumbar lymph node, which was significantly decreased at 6 weeks and 3 months after treatment. CT showed a reduction in lesion mass by 65 % and 80 % at 6 weeks and 3 months after RIT, respectively. At 6 months after RIT, FDG PET imaging indicated disease progression, but CT still showed a substantial reduction in lesion mass (84 %).

In addition to CD20 and CD22, several other biomarkers have been investigated as targets for RIT in lymphoma, including the human leukocyte antigen DR (HLA-DR) [127–129], CD21 [130, 131], and CD37 [132, 133]. In the past decade, HLA-DR has been extensively studied in the preclinical setting as a potential target for RIT. In a recent study, DeNardo et al. linked two small molecules known to interact with HLA-DR to mimic the targeting ability of an HLA-DR antibody [134]. The ^{64}Cu-labeled tracer was injected into xenograft-bearing mice and showed high specific uptake in lymphoma tumors expressing HLA-DR, while minimal uptake was seen in the HLA-DR-negative tumor model. In the future, the detection of new biomarkers and antibodies may significantly advance the field of RIT. For more information about RIT of lymphoma, readers are directed to some comprehensive reviews on this topic [135–137].

Discussion and future perspectives

Lymphoma is a difficult disease to diagnose due to its multifaceted pathology, which can easily be mistaken for other inflammatory and nonhematological diseases [138]. For this reason, physicians and researchers rely on several factors to accurately diagnose and study

the disease, including clinical history, morphology, phenotype, and genetics. While information regarding tumor phenotype can be obtained through immunohistochemistry and flow cytometry, highly invasive biopsies are required to retrieve the tissue for analysis. Substantial efforts have been devoted to methods for noninvasively assessing tumor phenotype in patients. Molecular imaging has been at the forefront of this field during the last decade, and provides the ability to noninvasively image tumors using designable imaging agents. PET is ideally suited for molecular imaging due to its high sensitivity and high resolution, and because it is not limited by tissue penetration depth [139]. Also, designing PET imaging agents has become simpler through advances in radiochemistry and isotope development.

In the future, PET imaging with radiolabeled antibodies may be used to select patients more likely to benefit from certain targeted therapies or it may provide insight into why certain patients experience treatment failure. Knowledge of the tumor phenotype from noninvasive imaging could allow optimization of treatment for individual patients. For example, PET imaging with an anti-CD20 tracer could be used to image a patient in whom anti-CD20 RIT has failed, and would provide an insight into the reason for treatment failure and assist in determining an alternative effective treatment plan.

With the cost of drugs rising each year, antibody-based imaging could become common practice before treating patients with expensive biological drugs that may be ineffective. As of 2016, the cost of Zevalin therapy is approximately $30,000, which is significantly cheaper than the cost of newer therapeutic antibodies. For example, two newer immunotherapeutic antibodies targeting programmed cell death protein 1 (nivolumab) and cytotoxic T-lymphocyte-associated protein 4 (ipilimumab) cost between $100,000 and $150,000 for a single course of therapy. It has been shown that both of these biomarkers are overexpressed in many types of lymphoma [140, 141]. Thus these antibodies may find a role in lymphoma imaging or RIT in the future. In 2016, the FDA approved nivolumab for the treatment of HL [142]. The potential of immune checkpoint inhibitor antibodies for tracking of activated T cells has been demonstrated in vivo [143], and this could be translated for imaging of lymphoma. For more information on molecular imaging of immunotherapy targets, readers are directed to our recent review of this topic [144].

While CD20 and CD30 are excellent biomarkers for antibody-targeted imaging, imaging agents targeting these entities often fall short in the preclinical and clinical settings. The most successful imaging agents, such as ^{18}F-FDG, show specificity towards several tumors and consistently provide excellent tumor visualization. Due to the natural specificity of antibodies, antibody tracers are good agents for cancer imaging, but they are readily limited by their lack of versatility. Unlike ^{18}F-FDG, antibody tracers target a single antigen, which may be differentially expressed among tumors of the same type. While CD20 and CD30 are effectively targeted by antibody tracers, newer dual-targeted imaging agents may improve the potential clinical usefulness of antibody-based radiotracers. In addition to the specificity, antibody tracers are also limited by their long circulation half-life and potential immunogenicity. For this reason, investigation of non-antibody imaging agents targeting CD20, CD30, and other lymphoma biomarkers, remains relevant. For example, Natarajan et al. engineered a novel anti-CD20 protein from the 10-kDa human fibronectin type 3 (FN3)

domain of CD20 [145]. The protein was radiolabeled ^{64}Cu and injected into CD20-expressing Ramos tumor-bearing mice. For comparison, tumor uptake was evaluated in mice receiving ^{64}Cu-labeled FN3 (16.8 ± 1.6 %ID/g) and ^{64}Cu-labeled rituximab (5.6 ± 1.4 %ID/g) at 1 h after injection, and showed that the small protein-based imaging agent may be well-suited for molecular imaging of B cell NHL at early time points after injection.

Currently, there are few studies that have investigated other potential biomarkers for imaging of lymphoma, yet the discovery of new biomarkers may provide additional benefits for imaging and therapeutic applications. In this regard, there have been some studies showing that CD5 and Forkhead box protein P1 (FOXP1) expression may be useful for predicting disease prognosis in patients with diffuse large B cell lymphoma [146, 147]. Hence, imaging of these biomarkers would provide added benefit at the time of diagnosis. In another study, the intensity of ^{18}F-FDG uptake in lymphomas was directly correlated with Glut1 expression in patients with HL and NHL [148]. Thus, identification of biomarkers expressed in more types of lymphoma may lead to the production of more clinically relevant imaging tools. In conclusion, radiolabeled antibodies have shown excellent potential for the noninvasive imaging of lymphoma in both preclinical animal models and patients; thus, with more research, these tracers may make excellent agents for the clinical imaging of lymphoma in the future.

Acknowledgments

Funding This work was funded, in part, by the University of Wisconsin–Madison, the National Institutes of Health (NIBIB/NCI 1R01CA169365, 1R01EB021336, P30CA014520, T32CA009206), and the American Cancer Society (125246-RSG-13-099-01-CCE).

References

1. Kuppers R. The biology of Hodgkin’s lymphoma. Nat Rev Cancer. 2009; 9(1):15–27. [PubMed: 19078975]
2. Engels EA. Infectious agents as causes of non-Hodgkin lymphoma. Cancer Epidemiol Biomarkers Prev. 2007; 16(3):401–404. [PubMed: 17337646]
3. Cerhan JR, Slager SL. Familial predisposition and genetic risk factors for lymphoma. Blood. 2015; 126(20):2265–2273. [PubMed: 26405224]
4. Campo E, Swerdlow SH, Harris NL, Pileri S, Stein H, Jaffe ES. The 2008 WHO classification of lymphoid neoplasms and beyond: evolving concepts and practical applications. Blood. 2011; 117(19):5019–5032. [PubMed: 21300984]
5. Swerdlow SH, Campo E, Pileri SA, et al. The 2016 revision of the World Health Organization classification of lymphoid neoplasms. Blood. 2016; 127(20):2375–2390. [PubMed: 26980727]
6. Swerdlow SH. Lymphoma classification and the tools of our trade: an introduction to the 2012 USCAP Long Course. Mod Pathol. 2013; 26(Suppl 1):S1–S14. [PubMed: 23281432]
7. Turner JJ, Hughes AM, Kricker A, et al. WHO non-Hodgkin’s lymphoma classification by criterion-based report review followed by targeted pathology review: an effective strategy for epidemiology studies. Cancer Epidemiol Biomarkers Prev. 2005; 14(9):2213–2219. [PubMed: 16172234]
8. Armitage JO. Early-stage Hodgkin’s lymphoma. N Engl J Med. 2010; 363(7):653–662. [PubMed: 20818856]
9. Dotan E, Aggarwal C, Smith MR. Impact of rituximab (Rituxan) on the treatment of B-cell non-Hodgkin’s lymphoma. Pharm Ther. 2010; 35(3):148–157.
10. Meng F, Zhong D, Zhang L, Shao Y, Ma Q. Efficacy and safety of rituximab combined with chemotherapy in the treatment of diffuse large B-cell lymphoma: a meta-analysis. Int J Clin Exp Med. 2015; 8(10):17515–17522. [PubMed: 26770342]

11. Rukstalis DB. Treatment options after failure of radiation therapy – a review. Rev Urol. 2002; 4(Suppl 2):S12–S17. [PubMed: 16986006]
12. Khalil DN, Smith EL, Brentjens RJ, Wolchok JD. The future of cancer treatment: immunomodulation, CARs and combination immunotherapy. Nat Rev Clin Oncol. 2016; 13(5): 273–90. [PubMed: 26977780]
13. Zappasodi R, de Braud F, Di Nicola M. Lymphoma immunotherapy: current status. Front Immunol. 2015; 6:448–454. [PubMed: 26388871]
14. Kharfan-Dabaja MA, Hamadani M, Sibai H, Savani BN. Managing Hodgkin lymphoma relapsing after autologous hematopoietic cell transplantation: a not-so-good cancer after all. Bone Marrow Transplant. 2014; 49(5):599–606. [PubMed: 24442246]
15. Toma P, Granata C, Rossi A, Garaventa A. Multimodality imaging of Hodgkin disease and non-Hodgkin lymphomas in children. Radiographics. 2007; 27(5):1335–1354. [PubMed: 17848695]
16. Gobbi PG, Ferreri AJ, Ponzoni M, Levis A. Hodgkin lymphoma. Crit Rev Oncol Hematol. 2013; 85(2):216–237. [PubMed: 22867814]
17. Luminari S, Bellei M, Biasoli I, Federico M. Follicular lymphoma – treatment and prognostic factors. Rev Bras Hematol Hemoter. 2012; 34(1):54–9. [PubMed: 23049385]
18. Ferrer R. Lymphadenopathy: differential diagnosis and evaluation. Am Fam Physician. 1998; 58(6):1313–1320. [PubMed: 9803196]
19. Jung W, Trumper L. Differential diagnosis and diagnostic strategies of lymphadenopathy. Internist (Berl). 2008; 49(3):305–318. [PubMed: 18273586]
20. Wang H, Qiu LN, Wu M, et al. Secondary B-cell lymphoma diagnosed by fine-needle aspiration cytology and flow cytometry following penile carcinoma: a case report. Oncol Lett. 2016; 11(4): 2449–2452. [PubMed: 27073496]
21. Demurtas A, Accinelli G, Pacchioni D, et al. Utility of flow cytometry immunophenotyping in fine-needle aspirate cytologic diagnosis of non-Hodgkin lymphoma: a series of 252 cases and review of the literature. Appl Immunohistochem Mol Morphol. 2010; 18(4):311–22. [PubMed: 19247181]
22. Beaty MW, Geisinger KR. Hodgkin lymphoma: flow me? Cytojournal. 2005; 2(1):13. [PubMed: 16150141]
23. Zeppa P, Marino G, Troncone G, et al. Fine-needle cytology and flow cytometry immunophenotyping and subclassification of non-Hodgkin lymphoma: a critical review of 307 cases with technical suggestions. Cancer. 2004; 102(1):55–65. [PubMed: 14968418]
24. Maecker HT, McCoy JP, Nussenblatt R. Standardizing immunophenotyping for the human immunology project. Nat Rev Immunol. 2012; 12(3):191–200. [PubMed: 22343568]
25. Reichard KK, Robinett S. Detection of genetic translocations in lymphoma using fluorescence in situ hybridization. Methods Mol Biol. 2013; 999:189–202. [PubMed: 23666698]
26. Friedberg JW, Chengazi V. PETscans in the staging of lymphoma: current status. Oncologist. 2003; 8(5):438–447. [PubMed: 14530496]
27. Wu AM, Olafsen T. Antibodies for molecular imaging of cancer. Cancer J. 2008; 14(3):191–197. [PubMed: 18536559]
28. Abdel Gawad EA, Abu Samra MF, Talat AM. The utility of multidetector CT in detection and characterization of mesenteric lymphadenopathy with histopathological confirmation. Egypt J Radiol Nucl Med. 2016; 47(3):757–764.
29. Kwee TC, Kwee RM, Nievelstein RA. Imaging in staging of malignant lymphoma: a systematic review. Blood. 2008; 111(2):504–516. [PubMed: 17916746]
30. Barrington SF, Mikhaeel NG, Kostakoglu L, et al. Role of imaging in the staging and response assessment of lymphoma: consensus of the International Conference on Malignant Lymphomas Imaging Working Group. J Clin Oncol. 2014; 32(27):3048–3058. [PubMed: 25113771]
31. Kwee TC, Takahara T, Vermoolen MA, Bierings MB, Mali WP, Nievelstein RA. Whole-body diffusion-weighted imaging for staging malignant lymphoma in children. Pediatr Radiol. 2010; 40(10):1592–1602. [PubMed: 20676622]
32. Kwee TC, van Ufford HM, Beek FJ, et al. Whole-body MRI, including diffusion-weighted imaging, for the initial staging of malignant lymphoma: comparison to computed tomography. Invest Radiol. 2009; 44(10):683–690. [PubMed: 19724232]

33. Edwards CL, Hayes RL. Tumor scanning with 67Ga citrate. J Nucl Med. 1969; 10(2):103–105. [PubMed: 5784705]
34. Pinsky SM, Henkin RE. Gallium-67 tumor scanning. Semin Nucl Med. 1976; 6(4):397–409. [PubMed: 185721]
35. Andrews GA, Edwards CL. Tumor scanning with gallium 67. JAMA. 1975; 233(10):1100–1103. [PubMed: 1174162]
36. Adler S, Parthasarathy KL, Bakshi SP, Stutzman L. Gallium-67-citrate scanning for the localization and staging of lymphomas. J Nucl Med. 1975; 16(4):255–260. [PubMed: 1089769]
37. van Leeuwen-Stok AE, Schuurhuis GJ, Drager AM, Visser-Platier AW, Teule GJ, Huijgens PC. Effect of modulation of the transferrin receptor on gallium-67 uptake and cytotoxicity in lymphoma cell lines. Br J Cancer. 1996; 74(4):619–624. [PubMed: 8761380]
38. Horn NL, Ray GR, Kriss JP. Gallium-67 citrate scanning in Hodgkin's disease and non-Hodgkin's lymphoma. Cancer. 1976; 37(1):250–257. [PubMed: 1247959]
39. Cwikla JB, Buscombe JR, Thakrar DS, Irwin AG, Hilson AJ. 67Ga SPECT in detection of infection and inflammation. Nucl Med Rev Cent East Eur. 1999; 2(2):69–73. [PubMed: 14600918]
40. Kostakoglu L, Yeh SD, Portlock C, et al. Validation of gallium-67-citrate single-photon emission computed tomography in biopsy-confirmed residual Hodgkin's disease in the mediastinum. J Nucl Med. 1992; 33(3):345–350. [PubMed: 1740700]
41. Fuertes MJ, Estorch CM, Camacho MV, et al. SPECT-CT 67Ga studies in lymphoma disease. Contribution to staging and followup. Rev Esp Med Nucl. 2006; 25(4):242–249. [PubMed: 16827987]
42. Iagaru A, Goris ML, Gambhir SS. Perspectives of molecular imaging and radioimmunotherapy in lymphoma. Radiol Clin N Am. 2008; 46(2):243–252. [PubMed: 18619379]
43. Paul R. Comparison of fluorine-18-2-fluorodeoxyglucose and gallium-67 citrate imaging for detection of lymphoma. J Nucl Med. 1987; 28(3):288–292. [PubMed: 3469332]
44. Hoh CK, Glaspy J, Rosen P, et al. Whole-body FDG-PET imaging for staging of Hodgkin's disease and lymphoma. J Nucl Med. 1997; 38(3):343–348. [PubMed: 9074514]
45. Kostakoglu L, Leonard JP, Kuji I, Coleman M, Vallabhajosula S, Goldsmith SJ. Comparison of fluorine-18 fluorodeoxyglucose positron emission tomography and Ga-67 scintigraphy in evaluation of lymphoma. Cancer. 2002; 94(4):879–88. [PubMed: 11920454]
46. Bar-Shalom R, Yefremov N, Haim N, et al. Camera-based FDG PET and 67Ga SPECT in evaluation of lymphoma: comparative study. Radiology. 2003; 227(2):353–60. [PubMed: 12637679]
47. Yang CC, Sun SS, Lin CC, Kao CH, Lee CC. Comparison of technetium-99m tetrofosmin and gallium-67 citrate scintigraphy for detecting malignant lymphoma. Anticancer Res. 2001; 21(5): 3695–3698. [PubMed: 11848545]
48. Shen YY, Kao A, Yen RF. Comparison of 18F-fluoro-2-deoxyglucose positron emission tomography and gallium-67 citrate scintigraphy for detecting malignant lymphoma. Oncol Rep. 2002; 9(2):321–325. [PubMed: 11836600]
49. Talbot JN, Haioun C, Rain JD, et al. [18F]-FDG positron imaging in clinical management of lymphoma patients. Crit Rev Oncol Hematol. 2001; 38(3):193–221. [PubMed: 11369254]
50. Kostakoglu L, Coleman M, Leonard JP, Kuji I, Zoe H, Goldsmith SJ. PET predicts prognosis after 1 cycle of chemotherapy in aggressive lymphoma and Hodgkin's disease. J Nucl Med. 2002; 43(8):1018–1027. [PubMed: 12163626]
51. Mikhaeel NG, Hutchings M, Fields PA, O'Doherty MJ, Timothy AR. FDG-PET after two to three cycles of chemotherapy predicts progression-free and overall survival in high-grade non-Hodgkin lymphoma. Ann Oncol. 2005; 16(9):1514–1523. [PubMed: 15980161]
52. Langer A. A systematic review of PET and PET/CT in oncology: a way to personalize cancer treatment in a cost-effective manner? BMC Health Serv Res. 2010; 10(1):283. [PubMed: 20932288]
53. Girinsky T, Auperin A, Ribrag V, et al. Role of FDG-PET in the implementation of involved-node radiation therapy for Hodgkin lymphoma patients. Int J Radiat Oncol Biol Phys. 2014; 89(5): 1047–1052. [PubMed: 25035208]

54. Rahmouni A, Luciani A, Itti E. MRI and PET in monitoring response in lymphoma. Cancer Imaging. 2005; 5(Spec No A):S106–S112. [PubMed: 16361125]
55. Haldorsen IS, Espeland A, Larsson EM. Central nervous system lymphoma: characteristic findings on traditional and advanced imaging. Am J Neuroradiol. 2011; 32(6):984–992. [PubMed: 20616176]
56. Carter BW, Wu CC, Khorashadi L, et al. Multimodality imaging of cardiothoracic lymphoma. Eur J Radiol. 2014; 83(8):1470–1482. [PubMed: 24935137]
57. Stephane V, Samuel B, Vincent D, et al. Comparison of PET-CT and magnetic resonance diffusion weighted imaging with body suppression (DWIBS) for initial staging of malignant lymphomas. Eur J Radiol. 2013; 82(11):2011–7. [PubMed: 23932096]
58. Akay S, Kocaoglu M, Emer O, Battal B, Arslan N. Diagnostic accuracy of whole-body diffusion-weighted magnetic resonance imaging with 3.0 T in detection of primary and metastatic neoplasms. J Med Imaging Radiat Oncol. 2013; 57(3):274–282. [PubMed: 23721135]
59. Palomero T, Ferrando AA. Genomic tools for dissecting oncogenic transcriptional networks in human leukemia. Leukemia. 2009; 23(7):1236–1242. [PubMed: 19158827]
60. Johnson NA, Savage KJ, Ludkovski O, et al. Lymphomas with concurrent BCL2 and MYC translocations: the critical factors associated with survival. Blood. 2009; 114(11):2273–2279. [PubMed: 19597184]
61. Li S, Lin P, Young KH, Kanagal-Shamanna R, Yin CC, Medeiros LJ. MYC/BCL2 double-hit high-grade B-cell lymphoma. Adv Anat Pathol. 2013; 20(5):315–326. [PubMed: 23939148]
62. Battey J, Moulding C, Taub R, et al. The human c-myc oncogene: structural consequences of translocation into the IgH locus in Burkitt lymphoma. Cell. 1983; 34(3):779–787. [PubMed: 6414718]
63. Ott G, Rosenwald A, Campo E. Understanding MYC-driven aggressive B-cell lymphomas: pathogenesis and classification. Blood. 2013; 122(24):3884–3491. [PubMed: 24009228]
64. Taub R, Kirsch I, Morton C, et al. Translocation of the c-myc gene into the immunoglobulin heavy chain locus in human Burkitt lymphoma and murine plasmacytoma cells. Proc Natl Acad Sci U S A. 1982; 79(24):7837–7841. [PubMed: 6818551]
65. Harris AW, Pinkert CA, Crawford M, Langdon WY, Brinster RL, Adams JM. The E mu-myc transgenic mouse. A model for high-incidence spontaneous lymphoma and leukemia of early B cells. J Exp Med. 1988; 167(2):353–371. [PubMed: 3258007]
66. Sheppard RD, Samant SA, Rosenberg M, Silver LM, Cole MD. Transgenic N-myc mouse model for indolent B cell lymphoma: tumor characterization and analysis of genetic alterations in spontaneous and retrovirally accelerated tumors. Oncogene. 1998; 17(16):2073–2085. [PubMed: 9798678]
67. Kovalchuk AL, Qi CF, Torrey TA, et al. Burkitt lymphoma in the mouse. J Exp Med. 2000; 192(8): 1183–1190. [PubMed: 11034608]
68. Yip KW, Reed JC. Bcl-2 family proteins and cancer. Oncogene. 2008; 27(50):6398–6406. [PubMed: 18955968]
69. Wang CG, Tai YH, Lisanti MP, Liao DJ. c-Myc induction of programmed cell death may contribute to carcinogenesis a perspective inspired by several concepts of chemical carcinogenesis. Cancer Biol Ther. 2011; 11(7):615–626. [PubMed: 21278493]
70. Kirkin V, Joos S, Zornig M. The role of Bcl-2 family members in tumorigenesis. Biochim Biophys Acta. 2004; 1644(2–3):229–249. [PubMed: 14996506]
71. Eischen CM, Woo D, Roussel MF, Cleveland JL. Apoptosis triggered by Myc-induced suppression of Bcl-X(L) or Bcl-2 is bypassed during lymphomagenesis. Mol Cell Biol. 2001; 21(15):5063–5070. [PubMed: 11438662]
72. Donnou S, Galand C, Touitou V, Sautes-Fridman C, Fabry Z, Fisson S. Murine models of B-cell lymphomas: promising tools for designing cancer therapies. Adv Hematol. 2012; 2012:701–704.
73. Kasama Y, Sekiguchi S, Saito M, et al. Persistent expression of the full genome of hepatitis C virus in B cells induces spontaneous development of B-cell lymphomas in vivo. Blood. 2010; 116(23): 4926–4933. [PubMed: 20733156]
74. Jinadasa R, Balmus G, Gerwitz L, Roden J, Weiss R, Duhamel G. Derivation of thymic lymphoma T-cell lines from Atm(−/−) and p53(−/−) mice. J Vis Exp. 2011; 50:2598.

75. Dranoff G. Experimental mouse tumour models: what can be learnt about human cancer immunology? Nat Rev Immunol. 2012; 12(1):61–66.
76. Klein AS, Plata F, Jackson MJ, Shin S. Cellular tumorigenicity in nude mice. Role of susceptibility to natural killer cells. Exp Cell Biol. 1979; 47(6):430–445. [PubMed: 520649]
77. Hanna N. The role of natural killer cells in the control of tumor growth and metastasis. Biochim Biophys Acta. 1985; 780(3):213–226. [PubMed: 3896313]
78. O'Connor OA, Toner LE, Vrhovac R, Budak-Alpdogan T, Smith EA, Bergman P. Comparative animal models for the study of lymphohematopoietic tumors: strengths and limitations of present approaches. Leuk Lymphoma. 2005; 46(7):973–992. [PubMed: 16019548]
79. Hunter RF, Roth PA, Huang AT. Cutaneous T cell lymphoma. Lymphocyte phenotype analysis after anti-thymocyte globulin therapy. Am J Med. 1985; 79(5):653–658. [PubMed: 3877463]
80. Imada K. Immunodeficient mouse models of lymphoid tumors. Int J Hematol. 2003; 77(4):336–341. [PubMed: 12774920]
81. Volpe R, Kasuga Y, Akasu F, et al. The use of the severe combined immunodeficient mouse and the athymic "nude" mouse as models for the study of human autoimmune thyroid disease. Clin Immunol Immunopathol. 1993; 67(2):93–99. [PubMed: 8519094]
82. Shimada K, Shimada S, Sugimoto K, et al. Development and analysis of patient-derived xenograft mouse models in intravascular large B-cell lymphoma. Leukemia. 2016; 30(7):1568–1579. [PubMed: 27001523]
83. Ito R, Takahashi T, Katano I, Ito M. Current advances in humanized mouse models. Cell Mol Immunol. 2012; 9(3):208–214. [PubMed: 22327211]
84. Shultz LD, Ishikawa F, Greiner DL. Humanized mice in translational biomedical research. Nat Rev Immunol. 2007; 7(2):118–130. [PubMed: 17259968]
85. Ali N, Flutter B, Sanchez Rodriguez R, et al. Xenogeneic graft-versus-host-disease in NOD-scid IL-2Rgammanull mice display a T-effector memory phenotype. PLoS One. 2012; 7(8):e44219. [PubMed: 22937164]
86. Covassin L, Jangalwe S, Jouvet N, et al. Human immune system development and survival of non-obese diabetic (NOD)-scid IL2rgamma(null) (NSG) mice engrafted with human thymus and autologous haematopoietic stem cells. Clin Exp Immunol. 2013; 174(3):372–388. [PubMed: 23869841]
87. Keating GM. Rituximab: a review of its use in chronic lymphocytic leukaemia, low-grade or follicular lymphoma and diffuse large B-cell lymphoma. Drugs. 2010; 70(11):1445–1476. [PubMed: 20614951]
88. Plosker GL, Figgitt DP. Rituximab: a review of its use in non-Hodgkin's lymphoma and chronic lymphocytic leukaemia. Drugs. 2003; 63(8):803–843. [PubMed: 12662126]
89. Barakzai MA, Pervez S. CD20 positivity in classical Hodgkin's lymphoma: diagnostic challenge or targeting opportunity. Indian J Pathol Microbiol. 2009; 52(1):6–9. [PubMed: 19136769]
90. Avivi I, Stroopinsky D, Katz T. Anti-CD20 monoclonal antibodies: beyond B-cells. Blood Rev. 2013; 27(5):217–223. [PubMed: 23953071]
91. Grillo-Lopez AJ, White CA, Varns C, et al. Overview of the clinical development of rituximab: first monoclonal antibody approved for the treatment of lymphoma. Semin Oncol. 1999; 26(5 Suppl 14):66–73.
92. Grillo-Lopez AJ, White CA, Dallaire BK, et al. Rituximab: the first monoclonal antibody approved for the treatment of lymphoma. Curr Pharm Biotechnol. 2000; 1(1):1–9. [PubMed: 11467356]
93. Natarajan A, Habte F, Gambhir SS. Development of a novel long-lived immunoPET tracer for monitoring lymphoma therapy in a humanized transgenic mouse model. Bioconjug Chem. 2012; 23(6):1221–1229. [PubMed: 22621257]
94. Zhang Y, Hong H, Cai W. PET tracers based on zirconium-89. Curr Radiopharm. 2011; 4(2):131–139. [PubMed: 22191652]
95. Natarajan A, Gambhir SS. Radiation dosimetry study of [(89)Zr]rituximab tracer for clinical translation of B cell NHL Imaging using positron emission tomography. Mol Imaging Biol. 2015; 17(4):539–547. [PubMed: 25500766]

96. Natarajan A, Habte F, Liu H, et al. Evaluation of 89Zr-rituximab tracer by Cerenkov luminescence imaging and correlation with PET in a humanized transgenic mouse model to image NHL. Mol Imaging Biol. 2013; 15(4):468–475. [PubMed: 23471750]

97. Natarajan A, Gowrishankar G, Nielsen CH, et al. Positron emission tomography of 64Cu-DOTA-rituximab in a transgenic mouse model expressing human CD20 for clinical translation to image NHL. Mol Imaging Biol. 2012; 14(5):608–616. [PubMed: 22231277]

98. Fontan C, Bezombes C, Salabert AS, et al. Radiolabelling rituximab with (99m)Tc in three steps procedure. J Labelled Comp Radiopharm. 2015; 58(7):274–280. [PubMed: 26017396]

99. Biffi S, Garrovo C, Macor P, et al. In vivo biodistribution and lifetime analysis of Cy5.5-conjugated rituximab in mice bearing lymphoid tumor xenograft using time-domain near-infrared optical imaging. Mol Imaging. 2008; 7(6):272–282. [PubMed: 19123997]

100. Olafsen T, Betting D, Kenanova VE, et al. Recombinant anti-CD20 antibody fragments for small-animal PET imaging of B-cell lymphomas. J Nucl Med. 2009; 50(9):1500–1508. [PubMed: 19690034]

101. Olafsen T, Sirk SJ, Betting DJ, et al. ImmunoPET imaging of B-cell lymphoma using 124I-anti-CD20 scFv dimers (diabodies). Protein Eng Des Sel. 2010; 23(4):243–249. [PubMed: 20053640]

102. Paudyal P, Paudyal B, Iida Y, et al. Dual functional molecular imaging probe targeting CD20 with PET and optical imaging. Oncol Rep. 2009; 22(1):115–119. [PubMed: 19513512]

103. Mendler CT, Friedrich L, Laitinen I, et al. High contrast tumor imaging with radio-labeled antibody Fab fragments tailored for optimized pharmacokinetics via PASylation. MAbs. 2015; 7(1):96–109. [PubMed: 25484039]

104. Younes A, Kadin ME. Emerging applications of the tumor necrosis factor family of ligands and receptors in cancer therapy. J Clin Oncol. 2003; 21(18):3526–3534. [PubMed: 12972530]

105. Durkop H, Foss HD, Eitelbach F, et al. Expression of the CD30 antigen in non-lymphoid tissues and cells. J Pathol. 2000; 190(5):613–618. [PubMed: 10727988]

106. Li P, Jiang L, Zhang X, Liu J, Wang H. CD30 expression is a novel prognostic indicator in extranodal natural killer/T-cell lymphoma, nasal type. BMC Cancer. 2014; 14:890. [PubMed: 25429803]

107. Sharman JP, Goldschmidt JH, Burke JM, Hellerstedt BA, McIntyre K, Yasenchak CA, et al. CD30 expression in nonlymphomatous malignancies. J Clin Oncol. 2012; 30(Suppl) abstract 3069.

108. Newland AM, Li JX, Wasco LE, Aziz MT, Lowe DK. Brentuximab vedotin: a CD30-directed antibody-cytotoxic drug conjugate. Pharmacotherapy. 2013; 33(1):93–104. [PubMed: 23307550]

109. Nagai H. Recent advances in Hodgkin lymphoma: interim PET and molecular-targeted therapy. J Clin Oncol. 2015; 45(2):137–145.

110. Schirrmann T, Steinwand M, Wezler X, Ten Haaf A, Tur MK, Barth S. CD30 as a therapeutic target for lymphoma. BioDrugs. 2014; 28(2):181–209. [PubMed: 24043362]

111. Kim W. Utilizing CD30 expression as a rational target for therapy of lymphoma. J Hematol Oncol. 2012; 5(Suppl 1):A2.

112. Engert A. CD30-positive malignant lymphomas: time for a change of management? Haematologica. 2013; 98(8):1165–1168. [PubMed: 23904233]

113. Moss A, Gudas J, Albertson T, Whiting N, Law C-L. Abstract 104: Preclinical microPET/CT imaging of 89Zr-Df-SGN-35 in mice bearing xenografted CD30 expressing and non-expressing tumors. Cancer Res. 2014; 74:104–109. [PubMed: 24197130]

114. Rylova SN, Del Pozzo L, Klingeberg C, et al. Immuno-PET imaging of CD30-positive lymphoma using 89Zr-desferrioxamine-labeled CD30-specific AC-10 antibody. J Nucl Med. 2016; 57(1): 96–102. [PubMed: 26514172]

115. Chamarthy MR, Williams SC, Moadel RM. Radioimmunotherapy of non-Hodgkin's lymphoma: from the 'magic bullets' to 'radioactive magic bullets'. Yale J Biol Med. 2011; 84(4):391–407. [PubMed: 22180677]

116. Iagaru A, Gambhir SS, Goris ML. 90Y-ibritumomab therapy in refractory non-Hodgkin's lymphoma: observations from 111In-ibritumomab pretreatment imaging. J Nucl Med. 2008; 49(11):1809–1812. [PubMed: 18927323]

117. Perk LR, Visser OJ, Stigter-van Walsum M, et al. Preparation and evaluation of (89)Zr-Zevalin for monitoring of (90)Y-Zevalin biodistribution with positron emission tomography. Eur J Nucl Med Mol Imaging. 2006; 33(11):1337–1345. [PubMed: 16832633]
118. Rizvi SN, Visser OJ, Vosjan MJ, et al. Biodistribution, radiation dosimetry and scouting of 90Y-ibritumomab tiuxetan therapy in patients with relapsed B-cell non-Hodgkin's lymphoma using 89Zr-ibritumomab tiuxetan and PET. Eur J Nucl Med Mol Imaging. 2012; 39(3):512–520. [PubMed: 22218876]
119. Muylle K, Flamen P, Vugts DJ, et al. Tumour targeting and radiation dose of radioimmunotherapy with (90)Y-rituximab in CD20+ B-cell lymphoma as predicted by (89)Zr-rituximab immuno-PET: impact of preloading with unlabelled rituximab. Eur J Nucl Med Mol Imaging. 2015; 42(8): 1304–1314. [PubMed: 25792453]
120. Larson SM, Carrasquillo JA, Cheung NK, Press OW. Radioimmunotherapy of human tumours. Nat Rev Cancer. 2015; 15(6):347–360. [PubMed: 25998714]
121. DeNardo GL. Treatment of non-Hodgkin's lymphoma (NHL) with radiolabeled antibodies (mAbs). Semin Nucl Med. 2005; 35(3):202–211. [PubMed: 16098294]
122. Davies AJ. Radioimmunotherapy for B-cell lymphoma: Y90 ibritumomab tiuxetan and I131 tositumomab. Oncogene. 2007; 26(25):3614–3628. [PubMed: 17530015]
123. Press OW, Unger JM, Rimsza LM, et al. Phase III randomized intergroup trial of CHOP plus rituximab compared with CHOP chemotherapy plus (131)iodine-tositumomab for previously untreated follicular non-Hodgkin lymphoma: SWOG S0016. J Clin Oncol. 2013; 31(3):314–320. [PubMed: 23233710]
124. Jovanovic D, Djurdjevic P, Andjelkovic N, Zivic L. Possible role of CD22, CD79b and CD20 expression in distinguishing small lymphocytic lymphoma from chronic lymphocytic leukemia. Contemp Oncol (Pozn). 2014; 18(1):29–33. [PubMed: 24876818]
125. Witzig TE, Tomblyn MB, Misleh JG, et al. Anti-CD22 90Y-epratuzumab tetraxetan combined with anti-CD20 veltuzumab: a phase I study in patients with relapsed/refractory, aggressive non-Hodgkin lymphoma. Haematologica. 2014; 99(11):1738–1745. [PubMed: 25150258]
126. Bodet-Milin C, Kraeber-Bodere F, Dupas B, et al. Evaluation of response to fractionated radioimmunotherapy with 90Y-epratuzumab in non-Hodgkin's lymphoma by 18F-fluorodeoxyglucose positron emission tomography. Haematologica. 2008; 93(3):390–397. [PubMed: 18268287]
127. DeNardo SJ, DeNardo GL, O'Grady LF, et al. Treatment of a patient with B cell lymphoma by I-131 LYM-1 monoclonal antibodies. Int J Biol Markers. 1987; 2(1):49–53. [PubMed: 3501448]
128. DeNardo GL, DeNardo SJ, Goldstein DS, et al. Maximum-tolerated dose, toxicity, and efficacy of I-131-Lym-1 antibody for fractionated radioimmunotherapy of non-Hodgkin's lymphoma. J Clin Oncol. 1998; 16(10):3246–3256. [PubMed: 9779698]
129. Pagel JM, Pantelias A, Hedin N, et al. Evaluation of CD20, CD22, and HLA-DR targeting for radioimmunotherapy of B-cell lymphomas. Cancer Res. 2007; 67(12):5921–5928. [PubMed: 17575162]
130. Czuczman MS, Straus DJ, Divgi CR, et al. Phase I dose-escalation trial of iodine 131-labeled monoclonal antibody OKB7 in patients with non-Hodgkin's lymphoma. J Clin Oncol. 1993; 11(10):2021–2029. [PubMed: 8410126]
131. Scheinberg DA, Straus DJ, Yeh SD, et al. A phase I toxicity, pharmacology, and dosimetry trial of monoclonal antibody OKB7 in patients with non-Hodgkin's lymphoma: effects of tumor burden and antigen expression. J Clin Oncol. 1990; 8(5):792–803. [PubMed: 2332769]
132. Press OW, Eary JF, Badger CC, et al. Treatment of refractory non-Hodgkin's lymphoma with radiolabeled MB-1 (anti-CD37) antibody. J Clin Oncol. 1989; 7(8):1027–1038. [PubMed: 2666588]
133. Kaminski MS, Fig LM, Zasadny KR, et al. Imaging, dosimetry, and radioimmunotherapy with iodine 131-labeled anti-CD37 antibody in B-cell lymphoma. J Clin Oncol. 1992; 10(11):1696–1711. [PubMed: 1403053]
134. DeNardo GL, Natarajan A, Hok S, et al. Pharmacokinetic characterization in xenografted mice of a series of first-generation mimics for HLA-DR antibody, Lym-1, as carrier molecules to image and treat lymphoma. J Nucl Med. 2007; 48(8):1338–1347. [PubMed: 17631545]

135. Juweid ME. Radioimmunotherapy of B-cell non-Hodgkin's lymphoma: from clinical trials to clinical practice. J Nucl Med. 2002; 43(11):1507–1529. [PubMed: 12411555]

136. Reagan PM, Friedberg JW. Advancing radioimmunotherapy and its future role in non-Hodgkin lymphoma. Future Oncol. 2015; 11(10):1543–1553. [PubMed: 25963431]

137. Bodet-Milin C, Ferrer L, Pallardy A, et al. Radioimmunotherapy of B-cell non-Hodgkin's lymphoma. Front Oncol. 2013; 3:177. [PubMed: 23875170]

138. Attanoos R. Lymphoproliferative conditions of the serosa. Arch Pathol Lab Med. 2012; 136(3): 268–276. [PubMed: 22372903]

139. Griffeth LK. Use of PET/CTscanning in cancer patients: technical and practical considerations. Proc (Bayl Univ Med Cent). 2005; 18(4):321–330. [PubMed: 16252023]

140. Yang ZZ, Grote DM, Ziesmer SC, Xiu B, Novak AJ, Ansell SM. PD-1 expression defines two distinct T-cell sub-populations in follicular lymphoma that differentially impact patient survival. Blood Cancer J. 2015; 5:e281. [PubMed: 25700246]

141. Xerri L, Devilard E, Hassoun J, Olive D, Birg F. In vivo expression of the CTLA4 inhibitory receptor in malignant and reactive cells from human lymphomas. J Pathol. 1997; 183(2):182–187. [PubMed: 9390031]

142. Ansell SM, Lesokhin AM, Borrello I, et al. PD-1 blockade with nivolumab in relapsed or refractory Hodgkin's lymphoma. N Engl J Med. 2015; 372(4):311–319. [PubMed: 25482239]

143. England CG, Ehlerding EB, Hernandez R, et al. Preclinical pharmacokinetics and biodistribution studies of 89Zr-labeled pembrolizumab. J Nucl Med. 2016; doi: 10.2967/jnumed.116.177857

144. Ehlerding EB, England CG, McNeel DG, Cai W. Molecular imaging of immunotherapy targets in cancer. J Nucl Med. 2016; 57(10):1487–1492. [PubMed: 27469363]

145. Natarajan A, Hackel BJ, Gambhir SS. A novel engineered anti-CD20 tracer enables early time PET imaging in a humanized transgenic mouse model of B-cell non-Hodgkins lymphoma. Clin Cancer Res. 2013; 19(24):6820–6829. [PubMed: 24097872]

146. Tzankov A, Leu N, Muenst S, et al. Multiparameter analysis of homogeneously R-CHOP-treated diffuse large B cell lymphomas identifies CD5 and FOXP1 as relevant prognostic biomarkers: report of the prospective SAKK 38/07 study. J Hematol Oncol. 2015; 8:70–77. [PubMed: 26071053]

147. Chuang WY, Chang H, Shih LY, et al. CD5 positivity is an independent adverse prognostic factor in elderly patients with diffuse large B cell lymphoma. Virchows Arch. 2015; 467(5):571–582. [PubMed: 26369546]

148. Khandani AH, Dunphy CH, Meteesatien P, Dufault DL, Ivanovic M, Shea TC. Glut1 and Glut3 expression in lymphoma and their association with tumor intensity on 18F-fluorodeoxyglucose positron emission tomography. Nucl Med Commun. 2009; 30(8):594–601. [PubMed: 19536037]

149. Swerdlow, SH., Campo, E., Harris, NL., Jaffe, ES., Pileri, SA., Stein, H., et al. WHO classification of tumours of haematopoietic and lymphoid tissues. Lyon: International Agency for Research on Cancer; 2008.

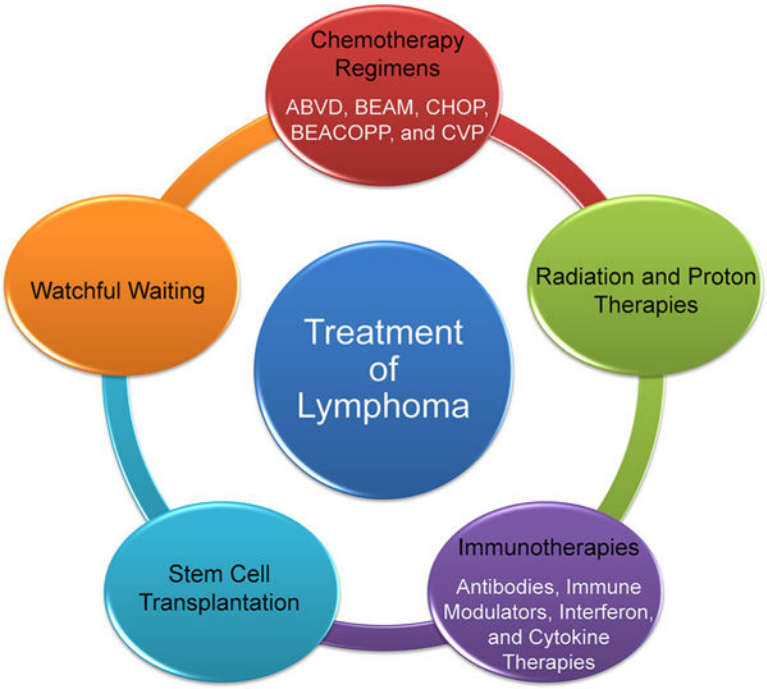

Fig. 1.

Strategies for the treatment of patients with lymphoma. Treatment may involve a combination of several modalities, including chemotherapy, radiation or proton therapy, immunotherapies, stem cell transplantation, or watchful waiting. There are several chemotherapeutic regimens for lymphoma, including ABVD (doxorubicin, bleomycin, vinblastine and dacarbazine), BEAM (carmustine, etoposide, cytarabine and melphalan), CHOP (cyclophosphamide, doxorubicin or hydroxydaunorubicin, vincristine and prednisone), BEACOPP (bleomycin, etoposide, doxorubicin, cyclophosphamide, vincristine, procarbazine and prednisolone), and CVP (cyclophosphamide, vincristine and prednisolone), and others. Immunotherapies may consist of monoclonal antibodies such as rituximab, proteasome inhibitors, immune modular (thalidomide and lenalidomide), targeted therapies, small molecule therapies (panobinostat), cytokine therapies, and interferon

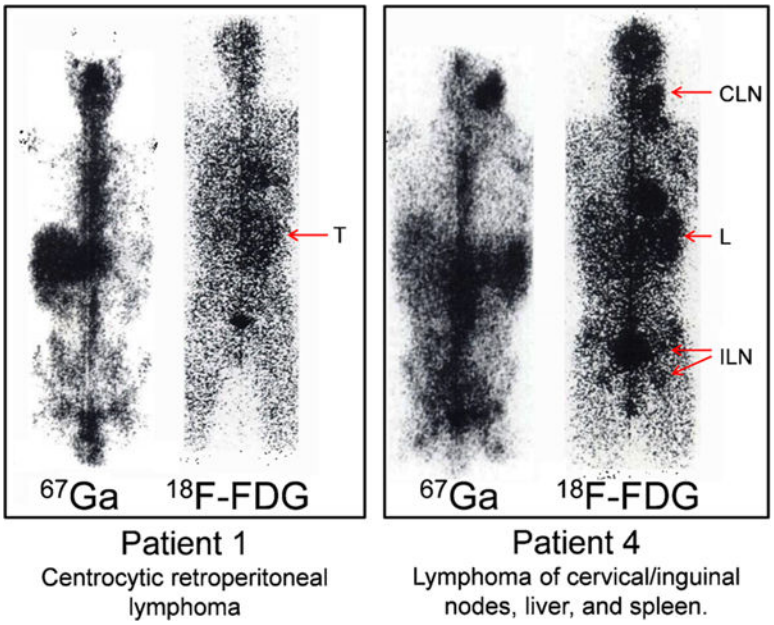

Fig. 2.

Comparison of ^{67}Ga and ^{18}F-FDG for imaging lymphoma. In *patient 1*, the ^{67}Ga scan is normal, while the ^{18}F-FDG scan clearly shows a lymphoma tumor (*T*) in the left quadrant of the retroperitoneum. In *patient 4*, lymphoma involvement in the inguinal lymph nodes (*ILN*) is visible on the ^{67}Ga scan, but is better delineated on the ^{18}F-FDG scan. Both scans show cervical lymph node (*CLN*) involvement, while the^{18}F-FDG scan shows liver (*L*) involvement. Reprinted with permission from Paul [43]

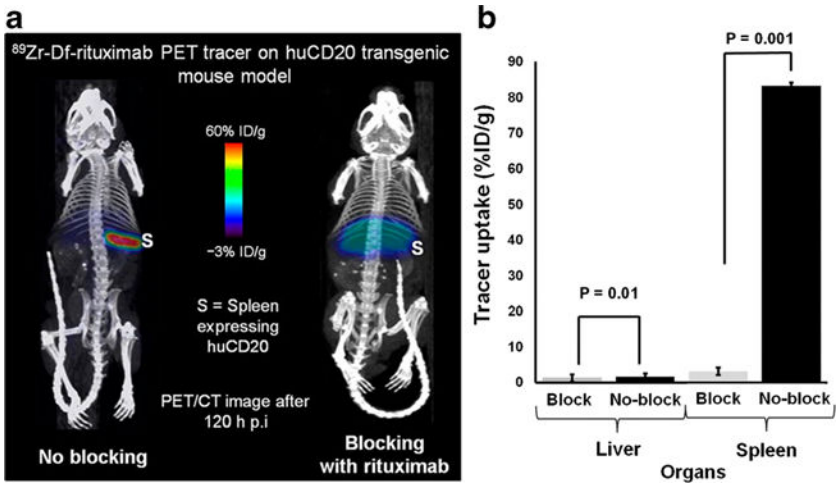

Fig. 3.

Imaging of CD20 expression in mice using ^{89}Zr-Df-rituximab. **a** PET/CT images 120 h after injection of ^{89}Zr-Df-rituximab into two groups of transgenic mice expressing human CD20 on their B cells. The mice of one group were injected directly with tracer, and the mice of the other group received a 2 mg/kg predose of rituximab to block the receptor. In the mouse without blocking (*left*), the spleen shows high uptake of tracer, and the mouse with blocking (*right*) shows minimal uptake of tracer (*S* spleen expressing human CD20). **b** Tracer uptake in the B cell-rich spleen was determined by region-of-interest analysis, and was found to be 83.3 ± 2.0 %ID/g in mice without blocking and 3.2 ± 0.1 %ID/g in mice with blocking at 120 h after injection. Low tracer uptake was found in the liver of both groups: 0.61 ± 0.001 % in mice without blocking and 1.32 ± 0.05 %ID/g in mice with blocking at 120 h after injection. Reprinted with permission [93]

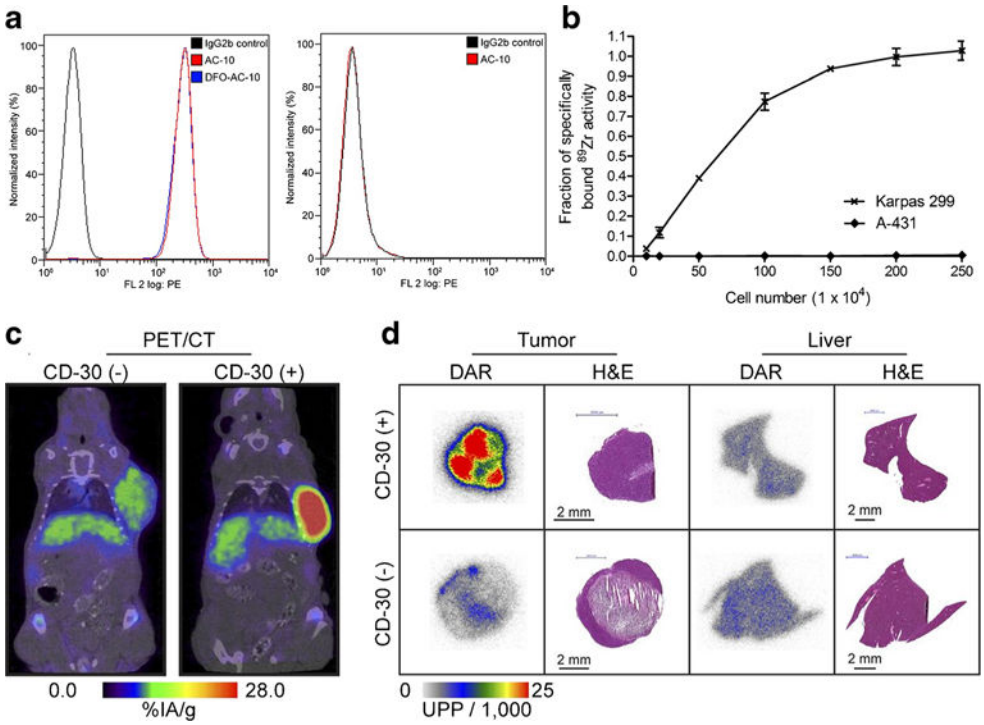

Fig. 4.

PET imaging of ^{89}Zr-DFO-AC-10 in CD30 expression in xenograft mice. **a** Flow cytometry was used to determine the binding specificity of AC-10 and DFO-AC-10 to CD30-positive Karpas 299 cells. The x-axis denotes that detector (FL2) was used to detect the dye (PE) and the data are shown in a log plot. **b** In vitro saturated binding assay of ^{89}Zr-DFO-AC-10 to CD30-positive Karpas 299 cells and CD30-negative A-431 cells. **c** PET/CT images of two representative mice bearing CD30-positive Karpas 299 and CD30-negative A-431 tumors at 144 h after injection. **d** Digital autoradiography and immunohistochemistry were used to evaluate the biodistribution of ^{89}Zr-DFO-AC-10 in tumor and liver of both mouse models (*H&E* hematoxylin and eosin, *DAR* digital autoradiography, *UPP* units per pixel). Reprinted with permission [114]

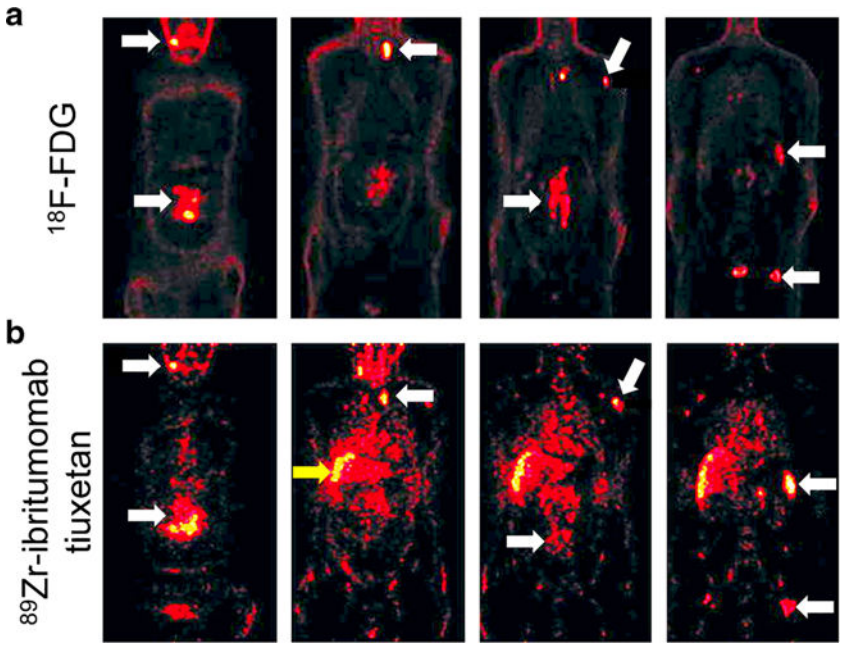

Fig. 5.

Comparison of ^{18}F-FDG and ^{89}Zr-ibritumomab tiuxetan PET imaging in a patient with NHL. **a** Coronal ^{18}F-FDG PET images obtained from the anterior (*left*) to the posterior (*right*). The cervical, mediastinal, splenic, left caput humeri, para-aortic, and inguinal lymph nodes are clearly visualized (*white arrows*). **b** ^{89}Zr-ibritumomab tiuxetan PET images obtained 96 h after tracer injection. The same lymphoma sites are visualized using this tracer (*white arrows*); however, liver uptake (*yellow arrow*) was attributed to the retention of ^{89}Zr after catabolism of the tracer. Reprinted with permission [117]

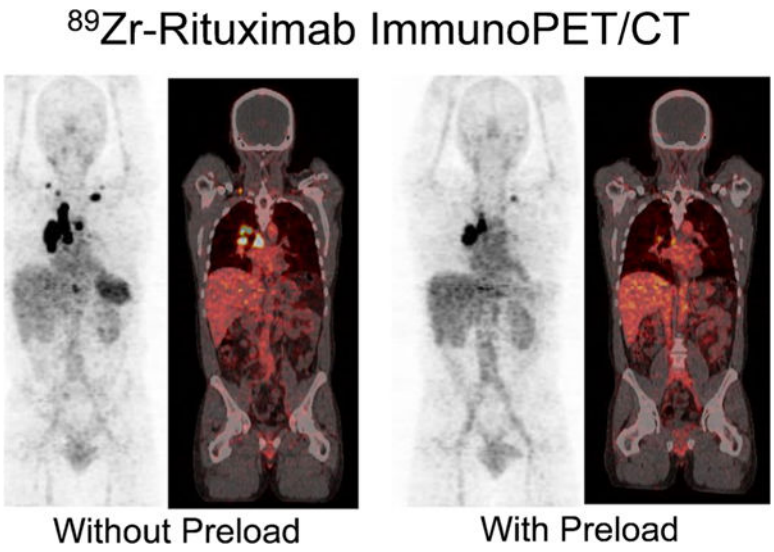

Fig. 6.

Biodistribution of ^{89}Zr-rituximab in an adult male with B cell-depleted grade II follicular lymphoma. PET/CT imaging was performed 6 days after injection of ^{89}Zr-Rituximab with or without a preload of unlabeled rituximab. Tumor targeting is higher without a preload of unlabeled rituximab. Reprinted with permission [119]

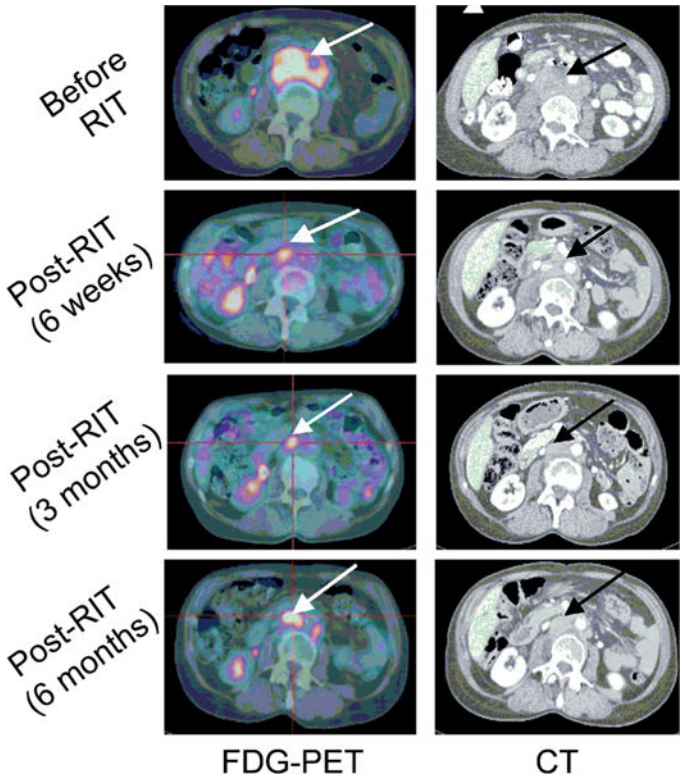

Fig. 7.

FDG PET for monitoring the response to RIT with ^{90}Y-epratuzumab. FDG PET and CT imaging were performed before and after RIT. Pretreatment images show the involvement of a lumbar lymph node (*arrow*). At 6 weeks and 3 months after treatment, the FDG PET images show a partial response. The CT images show a reduction in lesion mass by 65 % and 80 %, respectively. At 6 months after treatment, the FDG PET image indicates disease progression, while the CT image still shows a substantial reduction in lesion mass (84 %). Reprinted with permission [126]

Table 1

World Health Organization (WHO) classification of lymphoid neoplasms

Non-Hodgkin lymphoma				**Hodgkin lymphoma**	
B cell neoplasms		**T cell Neoplasms**		**Classical**	**Lymphocyte-predominant Hodgkin disease**
Precursor B cell neoplasms	**Mature B cell neoplasms**	**Precursor T cell neoplasms**	**Mature T cell and NK-cell neoplasms**		
Precursor B-lymphoblastic lymphoma	Small lymphocytic lymphoma	Precursor T-lymphoblastic lymphoma	T cell large granular lymphocytic leukemia	Nodular sclerosis Hodgkin lymphoma	Nodular lymphocyte-predominant Hodgkin lymphoma
	B cell prolymphocytic lymphoma		Adult T cell lymphoma	Mixed cellularity Hodgkin lymphoma	
	Splenic marginal zone lymphoma		Extranodal T cell lymphoma	Lymphocyte-rich Hodgkin lymphoma	
	Extranodal marginal zone B cell lymphoma		Enteropathy T cell lymphoma	Lymphocyte-depleted Hodgkin lymphoma	
	Lymphoplasmacytic lymphoma		Mycosis fungoides		
	Follicular lymphoma		Primary cutaneous T cell lymphoma		
	Mantle cell lymphoma		Systemic anaplastic large cell lymphoma		
	Diffuse large B cell lymphoma		Peripheral T cell lymphoma		
	Large B cell lymphoma		Hepatosplenic gamma/delta T cell lymphoma		
	Burkitt lymphoma		Aggressive NK-cell leukemia		
	Lymphomatoid granulomatosis		Blastic NK-cell lymphoma		

This table was adapted from Swerdlow et al. [149]

Table 2

FDG avidity for different types of lymphoma

Lymphoma type (WHO classification)	FDG avidity (%)	Number of patients
Hodgkin lymphoma	97 – 100	489
Follicular lymphoma	91 – 100	622
Diffuse large B cell lymphoma	97 – 100	446
Mantle-cell lymphoma	100	83
Burkitt's lymphoma	100	24
Anaplastic large T cell lymphoma	94 – 100	37
NK/T cell lymphoma	83 – 100	80
Peripheral T cell lymphoma	86 – 98	93
MALT marginal zone lymphoma	54 – 81	227
Mycosis fungoides	83 – 100	24
Small lymphocytic lymphoma	47 – 83	49
Marginal zone lymphoma, splenic	53 – 67	13
Marginal zone lymphoma, unspecified	67	12
Sézary syndrome	100	8
Primary cutaneous anaplastic large T cell lymphoma	40 – 60	14
Subcutaneous panniculitis-like T cell lymphoma	71	7
Cutaneous B cell lymphoma	0	2

Table adapted from Barrington et al. [30]

Table 3

Common lymphoma cell lines used for xenograft implantation in mice

Cell line	Cell type	Disease	Donor sex	Donor age
Karpas 299	T lymphocyte	Anaplastic large cell lymphoma	Male	25 years
SU-DHL-1	T lymphocyte	Anaplastic large cell lymphoma	Male	10 years
Daudi	B lymphoblast	Burkitt lymphoma	Male	16 years
Raji	B lymphocyte	Burkitt lymphoma	Male	11 years
H9 (from HuT 78)	T lymphocyte	Cutaneous T cell lymphoma	Male	53 years
HuT 102	T lymphocyte	Mycosis fungoides	Male	26 years
Pfeiffer	B lymphocyte	Diffuse large B cell lymphoma	Male	10 years
Toledo	B lymphocyte	Diffuse large B cell lymphoma	Female	Adult
Mino	B lymphocyte	Mantle cell lymphoma	Male	64 years
MAVER-1	B lymphocyte	Mantle cell lymphoma	Male	77 years
KM-H2	Reed-Sternberg	Hodgkin disease	Male	37 years
L540	Reed-Sternberg	Hodgkin disease	Female	20 years